Assessment of cloud optical parameters in the solar region: Retrievals from airborne measurements of scattering phase functions

Olivier Jourdan, Sergey Oshchepkov, Valery Shcherbakov, Jean-François Gayet, Harumi Isaka

Assessment of cloud optical parameters in the solar region: Retrievals from airborne measurements of scattering phase functions

Olivier Jourdan, Sergey Oshchepkov, Valery Shcherbakov, Jean-Francois Gayet, and Harumi Isaka

Laboratoire de Météorologie Physique (LaMP), Université Blaise Pascal, Clermont-Ferrand, France

Received 11 February 2003; revised 6 June 2003; accepted 27 June 2003; published 17 September 2003.

[1] A data set of approximately 60,000 airborne measurements of angular scattering coefficients was used to reproduce a representative set of both microphysical parameters and single light-scattering characteristics (angular scattering coefficient, asymmetry parameter, single-scattering albedo, and extinction coefficient) for three types of clouds. The measurements were limited to a wavelength of 0.8 μm and to 28 scattering angles near uniformly positioned from 15° to 155°. Microphysical and optical characteristics were computed at wavelengths of 0.8, 1.6, and 3.7 μm, which are needed for the direct and inverse modeling of radiative transfer. The estimation of these characteristics is achieved through cloud microphysical parameter retrievals, taking into account the variation of water droplet and ice crystal size as well as cloud phase composition. We present both average values and possible variability of microphysical and single-scattering characteristics for three types of clouds with respect to their particle phase composition (i.e., water droplets, mixed phase, and ice crystals in cloud). The variations are presented separately due to both random instrumental errors of optical measurements and possible changes in the microphysical parameters within a separated specific cloud category. The microphysical parameter retrievals are validated by comparison with collocated direct particle size distribution measurements. Additionally, the estimated single light-scattering characteristics are in reasonable agreement with those available from the literature. *INDEX TERMS:* 0320 Atmospheric Composition and Structure: Cloud physics and chemistry; 0649 Electromagnetics: Optics; 3260 Mathematical Geophysics: Inverse theory; 3359 Meteorology and Atmospheric Dynamics: Radiative processes; 3394 Meteorology and Atmospheric Dynamics: Instruments and techniques; *KEYWORDS:* cloud optical properties, inverse problem, radiative transfer

Citation: Jourdan, O., S. Oshchepkov, V. Shcherbakov, J.-F. Gayet, and H. Isaka, Assessment of cloud optical parameters in the solar region: Retrievals from airborne measurements of scattering phase functions, *J. Geophys. Res.*, *108*(D18), 4572, doi:10.1029/2003JD003493, 2003.

1. Introduction

[2] Scattering and absorption of short-wave and long-wave radiation by clouds affect the Earth's radiation balance [*Ramanathan et al.*, 1989]. In order to evaluate radiative effects such as climate forcing caused by clouds, an accurate characterization of the cloud optical and microphysical properties must be achieved [*Lacis and Mishchenko*, 1995; *Rossow and Schiffer*, 1999]. Moreover, satellite remote sensing techniques for the retrieval of physical and chemical properties of atmospheric particulates assume, in most cases, that optical properties should be adequately prescribed [see among others, *Kinne et al.*, 1992; *Rossow and Schiffer*, 1991]. In particular, *Liou and Takano* [1994] showed that retrievals of the optical depth and height of glaciated clouds using satellites' visible and infrared channels must use appropriate scattering phase functions for ice crystals. Nevertheless, "the convenient availability of the Lorenz-Mie solution has resulted in the widespread practice of treating nonspherical particles as if they were spheres..." [*Mishchenko et al.*, 2000]. Such simplification, however, can obviously cause significant biases in quantitative estimation of the particle's optical properties [*Mishchenko and Travis*, 2003]. Therefore more adequate modeling based on specific knowledge (measurements) of scattering and absorption characteristics of irregular particles is necessary. In order to validate parameterization of cloud single-scattering properties, comparison with in situ observations becomes essential [see among others, *Gonzalez et al.*, 2002].

[3] The previous statements assert that a large set of single-scattering characteristics for different types of clouds is required, for instance, for reliable inputs into climate models or for development of remote sensing techniques to infer cloud optical depth or hydrometeor size. Optical properties of cloud particles, as presented in the radiative transfer equations, can be summarized with their scattering phase function, extinction coefficient, single-scattering albedo, and asymmetry parameter. Spectral dependence of these param-

0148-0227/03/2003JD003493$09.00

eters also provides an important source of information to detect the phase of the cloud [*Liou et al.*, 2000]. In practice, no instrumental tool is capable of producing simultaneous measurements of such a range of parameters. Consequently, the missing characteristics are usually estimated on the basis of the measured ones.

[4] The estimated values can be computed directly, for example, on regression analysis grounds or indirectly through the retrieval of cloud microphysical parameters. The advantage of the indirect approach exists in the possibility to obtain the full set of the cloud single-scattering characteristics (subject to the condition that the satisfactory codes are available for the direct modeling). However, the main question is whether the initial experimental data set contains enough information with respect to the desired microphysical and optical parameters?

[5] The main goal of this study is to estimate representative and exploitable angular scattering coefficients (for scattering angles ranging from 0° to 180°) and single-scattering parameters in visible and infrared wavelengths using limited airborne "Polar Nephelometer" measurements. The estimation is achieved for different types of clouds relative to their particle phase composition (liquid-water phase; solid-ice phase, i.e., ice crystals; and mixed phase, i.e., water droplets and ice crystals). The measurements used in the study are based on the in situ angular scattering coefficient measurements performed with the Polar Nephelometer [*Gayet et al.*, 1997; *Crépel et al.*, 1997]. The experimental data have been obtained during three campaigns, namely, Avion de Recherche Atmosphérique et de Télédétection (ARAT'97) [*Duroure et al.*, 1998], CIRRUS'98 [*Durand et al.*, 1998], and the Japanese Cloud and Climate Study (JACCS'99) [*Asano et al.*, 2002; *Gayet et al.*, 2002a], which were carried out from Clermont-Ferrand (central part of France), Tarbes (southwest of France), and over the Sea of Japan, respectively. Collectively, these campaigns present the advantage of merging three large sets obtained in a wide variety of meteorological conditions.

[6] In our previous work [*Jourdan et al.*, 2003], a set of approximately 60,000 measured angular scattering coefficients was investigated. An objective data classification was performed in terms of cloud particle phase composition (water droplets, mixed phase, and ice crystals). For each cloud type, the average angular scattering coefficients (from 15° to 155°) were computed and the corresponding particle size distributions (PSDs) were retrieved. The retrievals were found to be in good agreement with the direct Particle Measuring Systems, Inc. (PMS) probe measurements.

[7] However, it should be noted that this work was restricted to nonpolarized light measurements due to the intrinsic optical setting of the Polar Nephelometer probe [see *Gayet et al.*, 1997]. Additionally, the measured angular scattering coefficient was limited to a wavelength of 0.8 μm and to near uniformly positioned 28 scattering angles from 15° to 155°.

[8] This paper is based on the limited angular scattering coefficients obtained in the previous work, presented by *Jourdan et al.* [2003], and intends to assess exploitable cloud optical and microphysical parameters for radiative transfer analysis.

[9] First, we introduce the necessary theoretical concepts regarding both direct physical modeling and the retrieval method. Then, for prescribed types of clouds, calculations are performed to extrapolate the average angular scattering coefficients (obtained from our previous work) to forward and backward scattering angles intervals ($\Theta < 15°$, $\Theta > 155°$) at the wavelength of 0.8 μm. The angular scattering coefficients are also investigated for wavelengths of 1.6 and 3.7 μm. Accordingly, the estimated average microphysical parameters and integral single light-scattering characteristics are presented for each cloud category and for the three wavelengths. Special attention is paid to variations in the retrieved parameters due to both random instrumental errors and possible changes of the cloud microphysical properties within a specific cloud category. Finally, we discuss the reliability of our results and their possible implementation in radiative transfer analysis.

2. Methodology and Theoretical Approach

[10] The Polar Nephelometer measures the angular light-scattering coefficient $\sigma(\Theta_j)$ of an ensemble of randomly oriented cloud particles as a function of specific light-scattering directions Θ_j. The measured angular scattering coefficient for a bicomponent cloud composed of particles with different phases and simple geometrical shapes (spheres, hexagonal crystals) can be expressed by the sum of integrals:

$$\sigma(\Theta_j) = \frac{3}{4}\sum_{s=1}^{2}\int_{-\infty}^{+\infty}\frac{Q_s(kR_s, \beta_s, m_s, \Theta_j)}{R_s}v_s(\ln R_s)d\ln R_s, \quad (1)$$

where the value of $\sigma(\Theta_j)$ is normalized through the total light-scattering coefficient σ_{sca} [μm^{-1}] as

$$\sigma_{sca} = 2\pi\int_0^{\pi}\sigma(\theta)\sin\theta\, d\theta, \quad (2)$$

with θ representing the scattering angle. It should be noted that the angular scattering coefficient, $\sigma(\theta)$ [μm^{-1} Sr^{-1}], is connected with the dimensionless normalized scattering phase function P_{11} as

$$\sigma(\theta) = \frac{P_{11}(\theta)}{4\pi}\sigma_{sca}. \quad (3)$$

Accordingly, the angular scattering coefficient could be considered and referred as a nonnormalized scattering phase function.

[11] In equation (1), the index $s = 1, 2$ stands for water droplets and ice crystals, respectively, $Q(kR, \beta_s, m_s, \Theta_j)$ is the light-scattering efficiency factor at a given scattering angle Θ_j for an individual particle with an equivalent radius R_s, an aspect ratio β_s, and a complex refractive index $m_s = n_s - i\chi_s$ at a specific wavelength, λ, included in the wave number definition: $k\ 2\pi/\lambda$. The equivalent size of an ice crystal is defined through the radius of an area-equivalent circle whose area is equal to the ice crystal cross section randomly oriented in 3-D space. In our calculations, the aspect ratio β_1 relative to the water droplet component is evidently equal to unity. On the other hand, the aspect ratio β_2 can vary but remains invariant for all sizes within the ice crystal particle size distribution.

[12] The volume distribution of particles introduced in equation (1) is defined by

$$v_s(\ln R_s) = \frac{dV_s}{d \ln R_s} = \frac{4}{3}\pi R_s^3 \frac{dN_s}{d \ln R_s}, \quad (4)$$

which satisfies the following normalized condition:

$$C_s = \int_{-\infty}^{+\infty} v_s(\ln R_s) d \ln R_s, \quad (5)$$

where C_s is the total volume content of each type of cloud particle per unit volume of the cloud. In equation (3), $\frac{dN_s}{d \ln R_s}$ is the particle number size distribution.

[13] Under sufficiently general conditions, equation (1) can be reduced to the set of linear algebraic equations

$$\boldsymbol{\sigma} = [\mathbf{K}_1 \mathbf{K}_2] \begin{bmatrix} \varphi_1 \\ \varphi_2 \end{bmatrix} + \Delta, \quad (6)$$

where σ is a column vector of measured values: $\{\sigma\}_j = \sigma(\Theta_j)$, φ_1 and φ_2 are column vectors with elements $\{\varphi_s\}_{i_s} = v_s(\ln R_{i_s})$ which correspond to the values of the volume distribution at different discrete sizes R_{i_s} for the sth component. The matrices $\mathbf{K}_s$ are defined through the efficiency factors $Q_s(kR_s, \beta_s, m_s, \Theta_j)$ whose elements are determined by the direct light-scattering model. In equation (6), Δ designates a column vector representing the random measurement errors (obeying the lognormal probability law in the following). Equation (6) can be rewritten in the more habitual form

$$\boldsymbol{\sigma} = \mathbf{K}\varphi + \Delta, \quad (7)$$

where the notations $\mathbf{K} = [\mathbf{K}_1 \mathbf{K}_2]$ and $\varphi = \begin{bmatrix} \varphi_1 \\ \varphi_2 \end{bmatrix}$ are used.

[14] The matrix elements of $\mathbf{K}_s$ are computed by linearly approximating the particle size distributions between points $\ln(R_{i_s+1})$ and $\ln(R_{i_s})$ and by interpolating between these points using a trapezoidal approximation according to *Twomey* [1977]:

$$\{\mathbf{K}_s\}_{ji} = \int_{\ln(R_{i_s})}^{\ln(R_{i_s+1})} \frac{\ln(R_{i_s+1}) - \ln R_s}{\ln(R_{i_s+1}) - \ln(R_{i_s})} \frac{Q_s(kR_s, \beta_s, m_s, \Theta_j)}{R_s} d \ln R_s + \int_{\ln(R_{i_s-1})}^{\ln(R_{i_s})} \frac{\ln R_s - \ln(R_{i_s-1})}{\ln(R_{i_s}) - \ln(R_{i_s-1})} \frac{Q_s(kR_s, \beta_s, m_s, \Theta_j)}{R_s} d \ln R_s \quad (8)$$

[15] In this case, the light-scattering efficiency factor $Q_s(kR_s, \beta_s, m_s, \Theta_j)$ is related to the phase function P_{11} and to the scattering coefficient, Q_{sca}, for a single particle of equivalent radius R_s by

$$Q_s(kR_s, \beta_s, m_s, \Theta_j) = \frac{P_{11}(kR_s, \beta_s, m_s, \Theta_j) Q_{\text{sca}}(kR_s, \beta_s, m_s)}{4\pi}. \quad (9)$$

[16] For specifying a lookup table, which contains scattering phase functions of individual ice crystals, we have limited ourselves by considering hexagonal ice crystals randomly oriented in 3-D space at a given aspect ratio for equivalent sizes ranging from 2 to 200 μm. While the scattering phase function of spherical water droplets obeys the Lorenz-Mie theory (for radius ranging from 0.5 to 50 μm), the scattering patterns of hexagonal crystals were computed by an improved geometric-optics model [*Yang and Liou*, 1996].

[17] In our recent paper [*Jourdan et al.*, 2003], we applied the above physical modeling to derive cloud microphysical properties using a statistical analysis of the angular scattering coefficients and inversion of equation (6). In a first step, the principal component analysis and a neural networks algorithm were implemented to the set of approximately 60,000 measured cloud angular scattering coefficients for 28 scattering directions ($15° \leq \Theta_j \leq 155°$) at a wavelength $\lambda = 0.8$ μm. This approach enables one to separate the set into three specific categories in terms of particle phase composition (i.e., water droplets, mixed phase, and ice crystals). For each class, a mean and a covariance matrix of the logarithm of the angular scattering coefficients were calculated. In a second step, the corresponding average angular scattering coefficients were used to retrieve both water and ice particle size distributions as inherent in each class. Then, the retrieval method developed by *Oshchepkov et al.* [2000] was used for the inversion. This method constitutes the nonlinear weighed least squares fitting of the angular scattering coefficient using positive and smoothness constraints on the desired particle size distributions. The positive constraints are achieved by implementation of the Gaussian statistics with respect to logarithm of both measured (σ) and desired (φ_1, φ_2) quantities [*Tarantola*, 1994]. The value of the aspect ratio β_2 for the ice crystal component is estimated on the basis of minimum residual between the measured and the retrieved angular scattering coefficient.

[18] We have shown that the retrievals were in good agreement with the average size composition obtained by independent direct particle size distribution data using the same set of collocated measurements. The statement is illustrated by the size distribution comparison presented in Figure 1. Such results lead to very important conclusions: (1) the Polar Nephelometer data carry enough information for appropriate retrieval of cloud component composition and particle size distributions and (2) the code used to calculate the optical parameters (in terms of angular scattering coefficients) is satisfactory. Accordingly, the obtained data, as expected, can be used for computing cloud single-scattering parameters at visible and infrared wavelengths.

[19] On the basis of the retrieved particle size distributions, the integrated optical parameters (asymmetry parameter, single-scattering albedo, and extinction coefficient), the extrapolated angular scattering coefficient at 0.8 μm as well as the angular scattering coefficients at other wavelengths are estimated for each type of clouds using the following scheme:

[20] A set of L estimated characteristics γ_l ($l = 1,2,\ldots,L$) can be computed from the retrieved particle size distribution $\hat{\varphi}$ with

$$\hat{\gamma} = \mathbf{G}\hat{\varphi}, \quad (10)$$

where $\hat{\gamma}$ is a vector column of γ_l, $\mathbf{G} = [\mathbf{G}_1 \mathbf{G}_2]$, and matrices $\mathbf{G}_1$ and $\mathbf{G}_2$ correspond to the efficiency factors of the estimated optical characteristics which are also linear func-

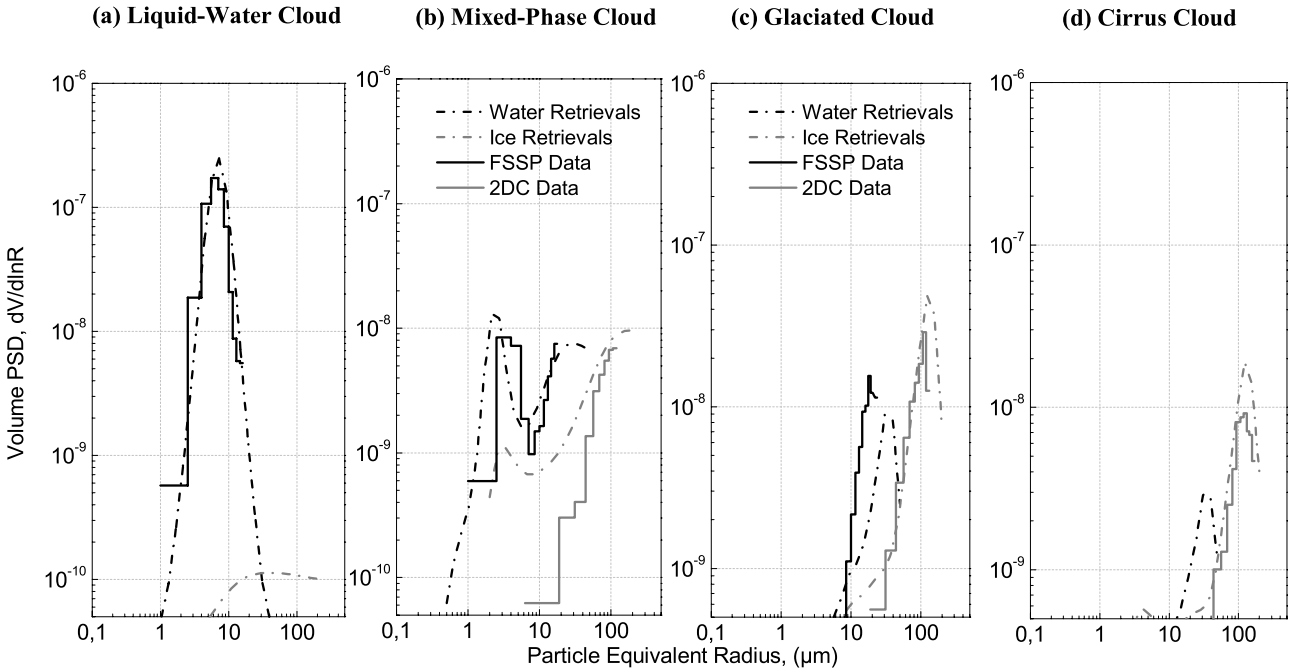

Figure 1. Inversion of the averaged angular scattering coefficients with respect to retrieval of both water droplets and ice crystal particle size distributions for four types of cloud: (a) water droplet cloud, (b) mixed-phase cloud, (c) ice crystal cloud, and (d) cirrus cloud. Direct particle size distributions (PMS probes) are indicated by histograms.

tions of primary parameters related to particle size distribution. The elements of matrix $\mathbf{G}_s$ are calculated following equation (8) but with the adequate efficiency factors corresponding to the desired quantity γ_l.

[21] Along with the retrievals, an important point lies in the analysis of variations of the retrieved parameters due to both random instrumental errors and possible changes of the cloud microphysical properties within a separated specific cloud category. The analysis of variations is achieved on the basis of covariance matrices $\mathbf{C}_\sigma$, $\mathbf{C}_\varphi$, and $\mathbf{C}_\gamma$ and is investigated in detail in Appendix A.

[22] As already mentioned above, both errors of the initial measurement and the retrievals were assumed to be described by the lognormal law, in a meaning of the probability density function, which is the most natural way to take a priori information about the nonnegativity of these quantities [*Tarantola*, 1994]. The simplest way to consider such a property is to turn the initial linear inverse problem into a nonlinear one in a normally distributed logarithmic space of σ. With such assumptions, equations (7)–(10) and equations (A1)–(A2) still remain valid but the quantities $\mathbf{C}_\sigma$, $\mathbf{C}_\varphi$, and $\mathbf{C}_\beta$ become the covariance matrices of logarithms of the measured angular scattering coefficient, retrieved PSD, and estimated optical characteristics, respectively. Therefore instead of the matrices $\mathbf{K}_s$ and $\mathbf{G}_s$, the Jacobian matrices $\mathbf{U}_s$ and $\mathbf{U}_s^*$ of the first derivatives in the near vicinity of the retrieved angular scattering coefficient should be used:

$$\{\mathbf{U}_s\}_{ji_s} = \partial(\ln \sigma_j)/\partial(\ln \varphi_{i_s}). \tag{11}$$

[23] Using the above formalism and the Polar Nephelometer data, we produce angular scattering coefficients extrapolated in the forward and backward light scattering directions ($\Theta_j < 15°$, $\Theta_j > 155°$) at $\lambda = 0.8$ μm, as well as at $\lambda = 1.6$ and 3.7 μm (the infrared region) applying equation (10). For each wavelength, the matrices $\mathbf{G}_s$ are determined by direct modeling from 0° to 180°, leading to fully described angular scattering coefficients. Equation (A2) is used to obtain the possible variations of the angular scattering coefficients within a particular cloud phase class. In addition, the single-scattering albedo, extinction coefficient, and asymmetry parameter are calculated for all three wavelengths (by means of equation (10)).

[24] The indicated two wavelengths in the infrared region are widely used by cloud space-borne radiometers (Moderate Resolution Imaging Spectroradiometer (MODIS), Global Imager (GLI), Along Track Scanning Radiometer (ATSR-2), Advanced Along Track Scanning Radiometer (AATSR)). All of these characteristics, along with the total water and ice volume density, are estimated for each type of cloud according to the classification made by *Jourdan et al.* [2003].

3. Results

[25] The ARAT'97, CIRRUS'98, and JACCS'99 experiments collected more than 60,000 synchronized optical and microphysical measurements with a spatial resolution of about 100 m. The microphysical cloud parameters (mainly, the particle size distributions) were inferred from measurements with an Forward Scattering Spectrometer Probe (FSSP-100), manufactured by PMS [*Knollenberg*, 1981] for water droplet diameters ranging from 3 to 45 μm and by the bidimensional optical array spectrometer PMS 2D-C probe [*Knollenberg*, 1981; *Gayet et al.*, 1996] for ice crystals, with a diameter size ranging from 25 to 800 μm. The optical data were obtained from angular scattering coefficients measurements performed by the

Table 1. Temperature Regimes and Retrieved and Measured Average Values of Microphysical Parameters for the Three Initial Types of Clouds and for the Cirrus Clouds[a]

Microphysical Parameters	Droplets and Crystals	Droplets	Crystals	Direct Measurements
Liquid-Water Clouds Temperature Interval: $-8°C < T < 5°C$; Mean Value $T = -4°C$				
Concentration, cm^{-3}	184.3	184.0	0.3	215
TWC, g m^{-3}	0.1618	0.1614	0.0004	0.1270
R_{eff}, μm	6.66	6.65	16.73	5.86
Mixed-Phase Clouds Temperature Interval: $-15°C < T < 0°C$; Mean Value $T = -7°C$				
Concentration, cm^{-3}	306.8	296.9	9.9	55.6
TWC, g m^{-3}	0.0345	0.0209	0.0137	0.0148
R_{eff}, μm	7.03	4.55	27.02	6.29
Solid-Ice (Glaciated) Clouds Temperature Interval: $-55°C < T < -3°C$; Mean Value $T = -14°C$				
Concentration, cm^{-3}	78.6	75.8	2.8	3.0
TWC, g m^{-3}	0.0384	0.0080	0.0304	0.024
R_{eff}, μm	38.1	12.8	70.8	32.4
Cirrus Clouds Temperature Interval: $-55°C < T < -40°C$; Mean Value $T = -45°C$				
Concentration, cm^{-3}	13.6	9.9	3.7	0.4
TWC, g m^{-3}	0.0159	0.0029	0.0130	0.0105
R_{eff}, μm	32.33	13.36	44.89	35.75

[a]For each of the temperature regimes, the retrieved parameters are presented for the water droplet part, the ice crystal part, as well as the total of both components.

Polar Nephelometer. The measurements involved different clouds types: stratocumulus, alto-cumulus, stratus, alto-stratus, cirro-stratus, and cirrus. On the basis of the neural network classification, average angular scattering coefficients and the corresponding particle size distributions were extracted. Nevertheless, classification was made on the basis of the cloud's phase and not on cloud type. So the glaciated phase (i.e., the solid-ice phase), for example, could involve not only cirrus cloud but also some regions in cirro-stratus, alto-stratus, alto-cumulus, or glaciated stratocumulus.

[26] The volume PSDs retrieved by the inversion method are presented along with those measured by the PMS FSSP-100 and 2D-C probes in Figure 1. The three first panels correspond to the three classes of particle phase composition ((1) liquid-water clouds, (2) mixed-phase clouds, and (3) solid-ice clouds). For each class, the curves "water retrievals" and "ice retrievals" present the PSDs retrieved for the water droplet component and for randomly oriented hexagonal ice crystals with aspect ratios equal to unity corresponding to minimum residuals, respectively. The labels "FSSP data" and "2DC data" indicate the corresponding direct PSD measurements (converted to particle volume size distribution).

[27] As mentioned above, the retrievals are in good agreement with direct measurements taking into account that all data are averaged. The Root-Mean-Square Devia-

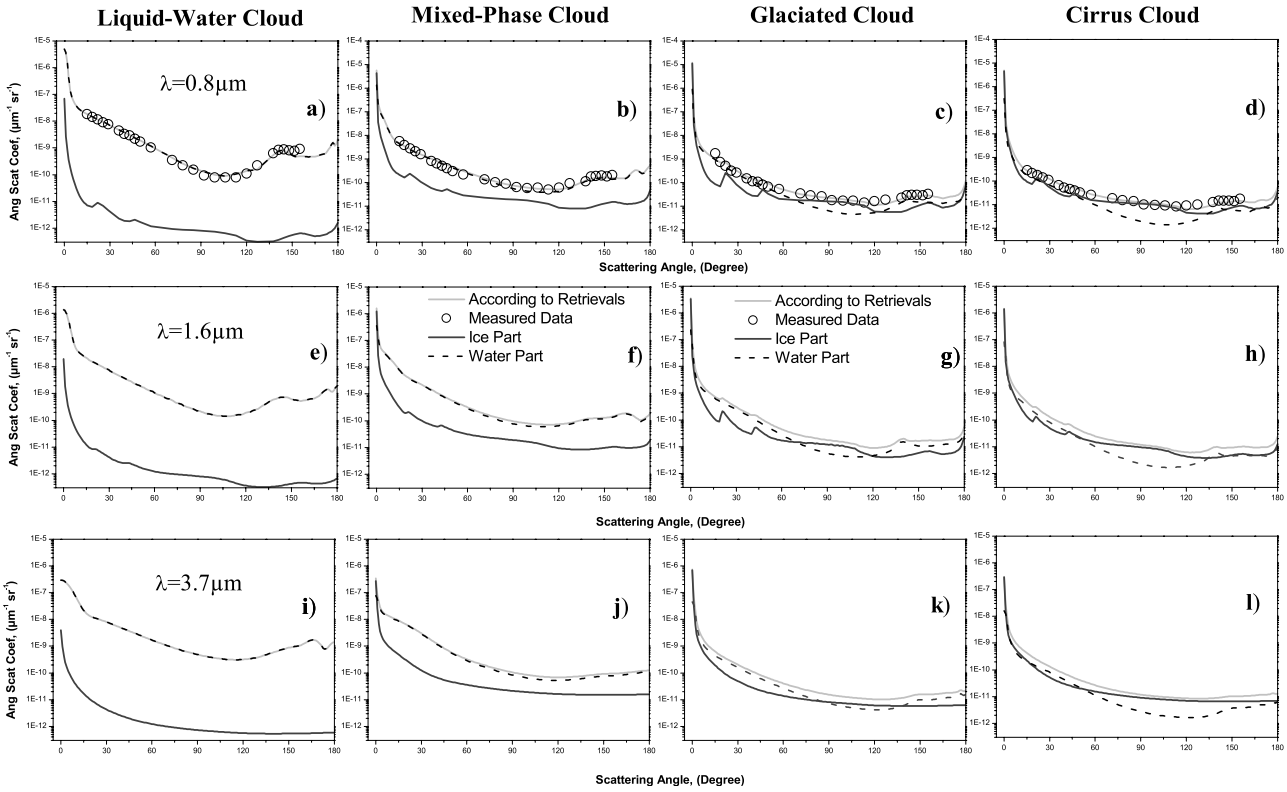

Figure 2. Extrapolation and projection of the angular scattering coefficients for the four types of cloud at three different wavelengths. The contributions on scattering properties are also displayed for both particle compositions (water and ice). (a, e, i) Water droplet cloud, (b, f, j) mixed-phase cloud, (c, g, k) ice crystal cloud, and (d, h, l) cirrus cloud. (Figures 2a, 2b, 2c, and 2d) $\lambda = 0.8$ μm, (Figures 2e, 2f, 2g, and 2h) $\lambda = 1.6$ μm, (Figures 2i, 2j, 2k, and 2l) $\lambda = 3.7$ μm.

tions (RMSD) between measured and retrieved angular scattering coefficients have minimum values when the aspect ratio of ice crystals is equal to one. The RMSD are calculated according to the definition used by *Oshchepkov and Isaka* [1997], giving acceptable values of 22, 24, and 21% for the water clouds, mixed-phase clouds, and glaciated clouds, respectively.

[28] The water droplet component dominates the ice crystal component (Figure 1a), and the PSD for these components have the same order of magnitude in the case of a mixed-phase cloud (Figure 1b). In Figure 1c, the crystals dominate the spherical droplets, although there is some disagreement between direct measurements and retrievals for small particles. It should be noted in this regard, that the 2D-C measurements present high uncertainties for an equivalent radius less than 50 μm [*Gayet et al.*, 2002b]. The relationship between the two components can be seen more clearly from the retrieved water content values of Table 1. The ratio (liquid water content)/(ice water content) is 455.4, 1.5, and 0.26 for the water droplets, mixed-phase, and ice crystals classes, respectively.

[29] The angular scattering coefficients estimated for the wavelengths 0.8, 1.6, and 3.7 μm are presented in Figure 2. For each cloud category, we also present here the angular scattering coefficients for water and ice separately. Figures 2a, 2b, and 2c correspond to $\lambda = 0.8$ μm; Figures 2e, 2f, and 2g correspond to $\lambda = 1.6$ μm; and Figures 2i, 2j, and 2k correspond to $\lambda = 3.7$ μm. Accordingly, Figures 2a, 2e, and 2i correspond to liquid-water clouds; Figures 2b, 2f, and 2j correspond to mixed-phase clouds; and Figures 2c, 2g, and 2k correspond to solid-ice clouds. The curve "according to retrievals" presents the "extrapolated" or corresponding "projected" angular scattering coefficients when both of the retrieved fractions are considered. The labels "water part" and "ice part" are used for the angular scattering coefficients, which are calculated only on the base of the retrieved PSD of spherical water droplets and randomly oriented hexagonal crystals, respectively.

[30] The angular scattering coefficient measurements as subject of the inversion are seen to be in good agreement with those computed according to the retrievals for all three types of clouds. The retrieved volume particle size distributions provide the extrapolation of the phase functions into forward ($\Theta < 15°$) and backward angles ($\Theta > 155°$) at the wavelength $\lambda = 0.8$ μm using equation (10). The effect of nonspherical particles (ice crystals) on the angular scattering coefficient is seen from Figure 2 to be negligible at all three wavelengths for the liquid-water cloud. For the mixed-phase case, the impact can be noticed at small forward and at sideward angles for $\lambda = 0.8$ μm and at angles greater then 60° for the wavelengths 1.6 and 3.7 μm. At the same time, the effect of spherical particles is not negligible for the glaciated cloud at all three wavelengths.

[31] The impact of instrumental errors and variation of microphysical parameters within a certain separated specific cloud category are presented separately and displayed in Figures 3, 4, and 5 for each class. The error bars are due to instrumental errors, which were also computed through diagonal elements of the covariance matrix $\mathbf{C}_\gamma$ according to equation (A2), with the difference that only the instrumental covariance matrix Σ was used instead of $\mathbf{C}_\sigma$. The instrumental errors were assumed not to be correlated, meaning that the

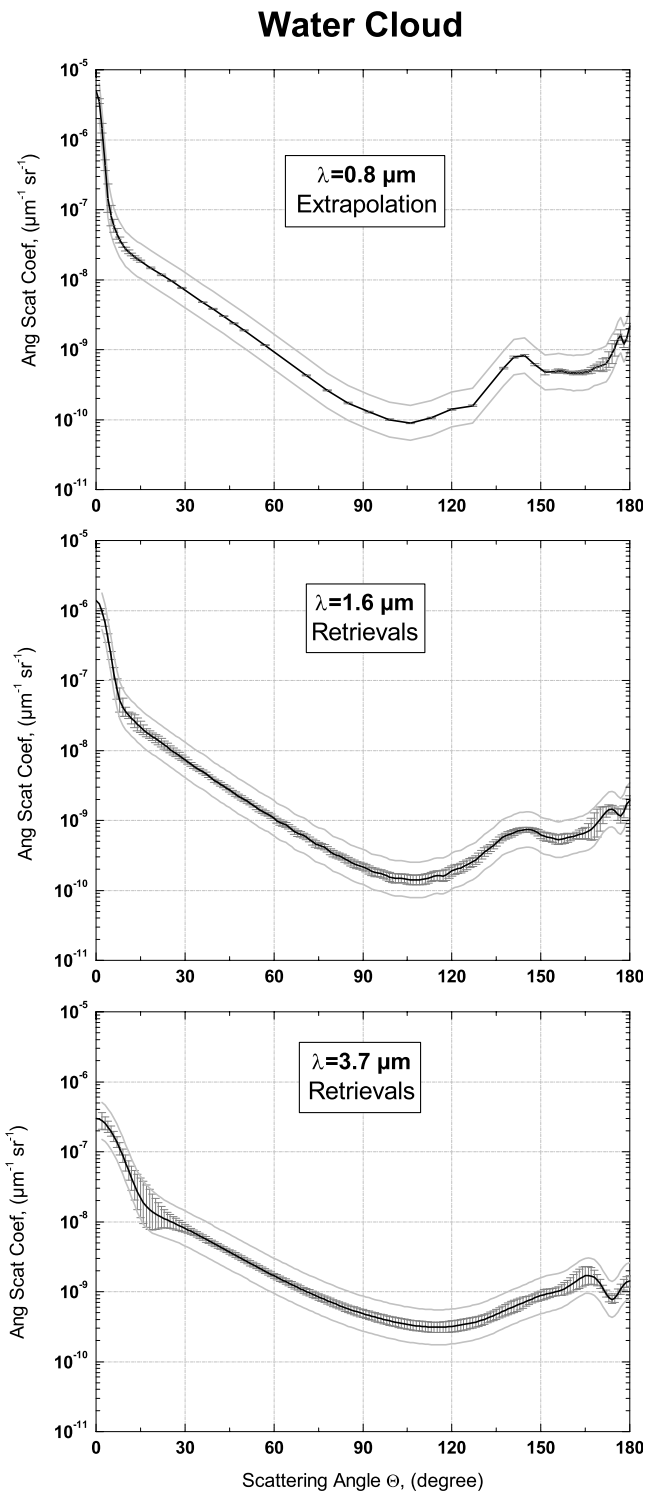

Figure 3. Average angular scattering coefficient (solid black line) and its variations caused by both instrumental errors (shaded error bars) and physical variations of microphysical parameters within each separated cloud category (upper and lower solid light shaded lines) presented for the three wavelengths. Case of water droplet cloud.

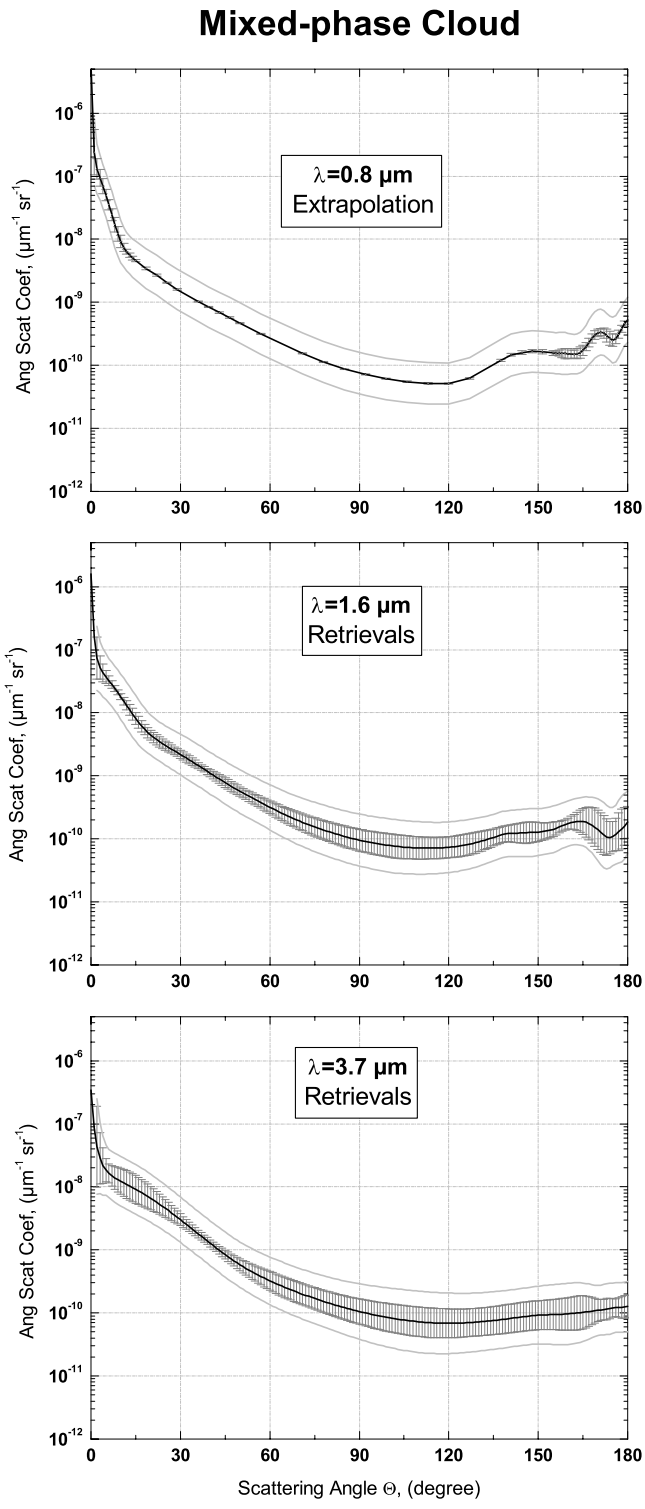

Figure 4. Same as in Figure 3 but for mixed-phase cloud.

matrix Σ has diagonal structure. The corresponding diagonal elements are defined on the basis of present knowledge on the relative instrumental error variance as a function of scattering angle Θ_j. A set of calibrations of the Polar Nephelometer were made to estimate the relative instrumental errors depending on the measurement channel. The errors are 3% for scattering angles ranging from 25.5° to 127°; 5% for forward scattering angles between 15° to 22°; and around 10% for backscattering angles between 144° and 155°.

[32] It seems quite reasonable that the error bars caused by instrumental noise are small for initial measurements (from 15° to 155° and $\lambda = 0.8$ μm). Beyond these scattering directions, the uncertainties are higher, especially for the mixed-phase and solid-ice clouds. For the forward directions, the result is explained by the fact that the measured

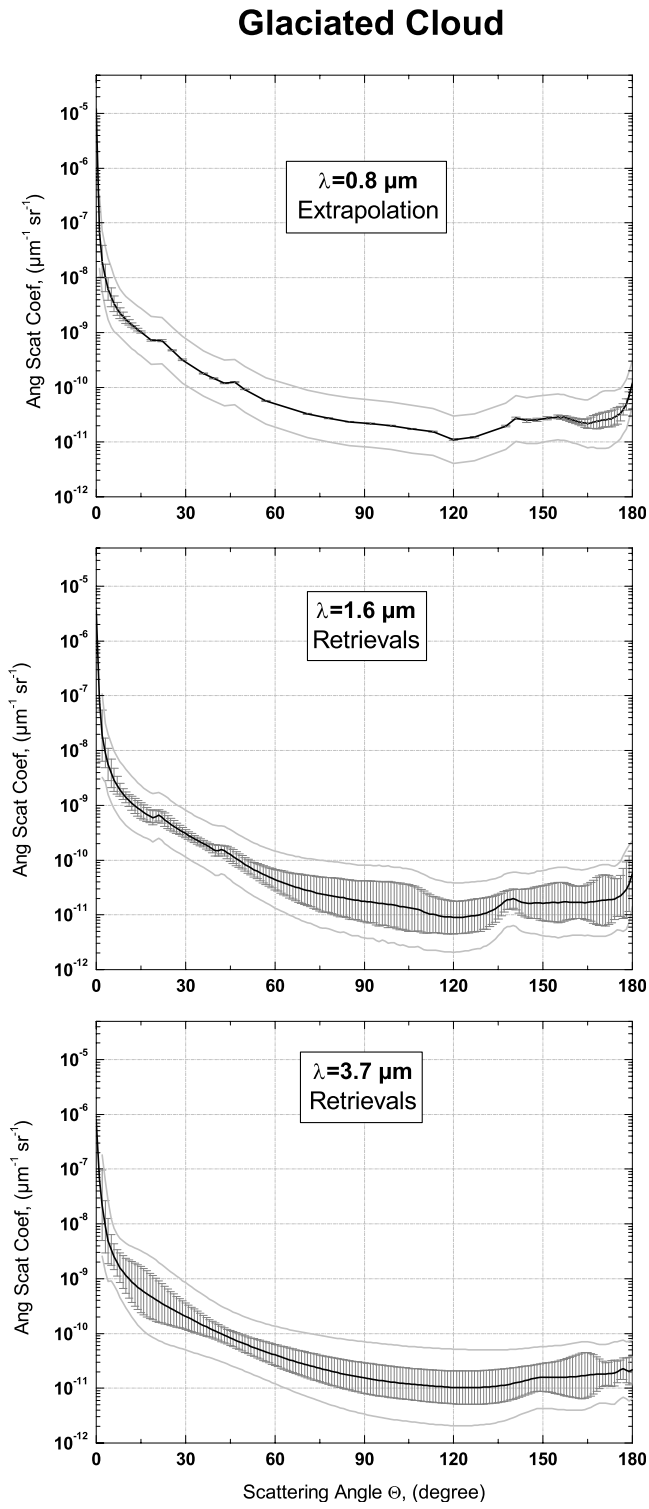

Figure 5. Same as in Figure 3 but for ice crystal cloud.

angular scattering coefficient carries a limited amount of information with respect to large particles.

[33] Accordingly, the relative errors of the retrieved optical parameters derived from the angular scattering coefficients caused by the instrumental noise are close to 2% for water droplet clouds but reach 4.5% for mixed-phase clouds and reach 6% in the case of glaciated clouds at 0.8 μm. For the infrared wavelengths 1.6 and 3.7 μm, the errors bars are on the same order of magnitude throughout all scattering angles, during which the error level is increased as the fraction of ice crystals increases. The explanation could be the same as mentioned above due to both a decrease in size parameters (sensitivity term $\mathbf{G}_l\mathbf{G}_l^T$ in equation (A3) becomes higher for the infrared region) and an increase in the ice crystal absorption properties.

[34] As pointed out above, variations in the computed optical characteristics caused by both changes of microphysical properties of clouds and instrumental errors are estimated by computing the diagonal elements of the covariance matrix $\mathbf{C}_\gamma$ with $\mathbf{C}_\sigma$ for each separated class of cloud. The angular scattering coefficient variations are also presented in Figures 3, 4, and 5. For simplicity sake, heavy light gray curves are used here instead of bars. Of course, the estimated angular scattering coefficient cannot vary arbitrarily because of the existing correlations between values at different angles. As expected, changes of microphysical properties of clouds lead to higher variability of estimated angular scattering coefficient relative to instrumental errors. As before, the higher the hexagonal ice crystals fraction, the higher the variations of the phase functions.

[35] The average microphysical parameters and integral single light-scattering characteristics are presented in Tables 1 and 2 and Tables 3 and 4, respectively. Shown are the volume extinction coefficient (σ_{ext}), the single-scattering albedo (ω_{sca}), the asymmetry parameter (g), the particle number concentration (Conc), the total water content (TWC = LWC + IWC, i.e., the sum of the liquid and ice water contents), and the cloud particle effective radius (R_{eff}) defined as the ratio of the third to second moment of the droplet-size distribution.

[36] For microphysical parameters, water and ice fractions and direct measurements are also presented in Table 1 as well as the temperature regimes for each type of cloud. Comparison between retrieved microphysical parameters and measurements shows that for all cloud cases, the effective radius and the total water content are accurately retrieved. The retrievals of concentration, however, except in the water cloud case, are not acceptable. It could be explained by the fact that the inversion scheme is more effective to retrieve the volume parameters because the Polar Nephelometer measurements correspond to volume scattering properties of an ensemble of sampled cloud particles. Furthermore, the retrieved microphysical parameters accurately reproduce cloud radiative properties, but not necessarily compare well with the "true" measured parameters. This point will be discussed in section 4.

[37] The maximum and minimum values of the optical parameters corresponding to the variations of microphysical parameters for each separated class are referenced in Tables 2, 3, and 4. The volume extinction coefficients $\sigma_{ext}(\lambda)$ have highest values for the water droplet class and lowest for the ice crystal class at all wavelengths. As expected, the single-scattering albedo is maximal at λ = 0.8 μm and minimal at λ = 3.7 μm. This is due to the spectral properties of the imaginary part of the refractive indexes of water and ice. It follows from Table 2 that for the water droplet class, the inequality σ_{ext} (0.8) < σ_{ext} (1.6) < σ_{ext} (3.7) is valid, the inverse wavelength dependence is seen for the ice crystals case, and the relationship σ_{ext} (0.8) < σ_{ext} (3.7) < σ_{ext} (1.6) takes place for the mixed-phase cloud. The asymmetry factors $g(\lambda)$ for the water and mixed-phase clouds offer the following properties: $g(3.7) < g(1.6) < g(0.8)$ and the inequality $g(3.7) < g(0.8) < g(1.6)$ takes place for the ice cloud.

Table 2. Retrieved Single-Scattering Properties for the Three Wavelengths Considering Mean, Maximum, and Minimum Possible Value Caused Physical Variations of Microphysical Parameters for Each Separated Type of Cloud[a]

Liquid-Water Clouds	Mean Value	Lowest Value	Highest Value
	$\lambda = 0.8$ μm		
Extinction: σ_{ext}, km^{-1}	39.347	22.071	70.152
Albedo: ω_{sca}	1.000	1.000	1.000
Asymmetry: g	0.8480	0.8477	0.8481
	$\lambda = 1.6$ μm		
Extinction: σ_{ext}, km^{-1}	41.222	23.040	73.762
Albedo: ω_{sca}	0.9952	0.9951	0.9952
Asymmetry: g	0.8275	0.8269	0.8282
	$\lambda = 3.7$ μm		
Extinction: σ_{ext}, km^{-1}	44.320	24.541	80.054
Albedo: ω_{sca}	0.9264	0.9254	0.9271
Asymmetry: g	0.7474	0.7420	0.7530

[a]Case of water droplet cloud.

[38] In order to be consistent with the already published values of the asymmetry parameter, the determination of g at all three wavelengths is done taking into account the effect of the δ function transmission through hexagonal ice crystals which occurs at $\theta = 0°$ when the opposite facets of the ice crystal are exactly parallel. The values of the asymmetry parameters presented in this work are already corrected following the method proposed by *Takano and Liou* [1989] and depend on the fraction of light transmitted at $\theta = 0°$ to the total scattered light.

[39] The spectral dependencies of the single-scattering parameters can be explained by the microphysical parameters of the retrieved particle size distributions and the relationships between the spherical droplet and the hexagonal ice crystal fractions. It is well known that there is a rather high correlation between single-scattering parameters and the particle effective radius R_{eff} of clouds. For the hexagonal ice crystal fraction, the value R_{eff} is much higher for the ice crystal class compared with others. At the same time, the effective radius of the spherical droplet fraction has a smaller value for the mixed-phase case.

4. Discussion and Comparison With Published Data

[40] In this study, we have postulated that for each type of cloud the inferred angular scattering coefficient corresponds to a combination of a water droplet component and a hexagonal ice crystal component. Optical parameters are

computed considering this statement. From a microphysical point of view, this hypothesis might not be correct, leading to erroneous retrieved microphysical parameters, but the aim of this study is to present realistic optical parameters for three types of clouds in order to improve radiative transfer code.

[41] However, we recall that the 2D-C probe does not reliably measure small ice crystals, so this could lead to a significant underestimate of the ice particle concentrations. The main disagreement between the retrieved microphysical parameters and the measured ones for mixed-phase and glaciated clouds concerned concentration retrievals, which could indeed be explained by this particular concentration underestimation. In section 3, it was shown that our microphysical model with a simple two-component assumption is sufficient to model angular scattering coefficients in agreement with the measurements. Moreover, the retrieved volume particle size distributions compared well with the ones obtained by direct measurements. These two results enable us to expect rather good accuracy in assessing representative cloud optical parameters in the solar region.

[42] Additionally, in situ measurements in glaciated clouds show a great variability in the size, shape, structure, and surface roughness of ice crystals. At the moment, no existing model is able to summarize such discrepancies. The most sophisticated ones include mathematical representations of crystal-shape complexities (see among others the Koch fractal polycrystals developed by *Macke et al.* [1996] and the hexagonal ice aggregates developed by *Yang and Liou* [1998]), surface roughness (imperfect hexagonal crystals by *Hess et al.* [1998]), and inhomogenity (inhomogeneous hexagonal model with internal inclusions by *Labonnote et al.* [2000]) in order to produce "realistic" optical behavior of ice clouds.

[43] The microphysical model used in this study is rather simple but remains flexible and sufficient to take into account cloud composition and size effects. Finally, the retrieval of cloud's optical properties lies within the framework of the inverse problem. The limited information content of the measured angular scattering coefficients prevents the accurate retrieval of numerous parameters characterizing complex ice crystal shapes or surface roughness. It only allows us to retrieve the cloud phase composition, its particle size distributions, and the aspect ratio of the assumed hexagonal ice crystals.

[44] Accordingly, the use of our microphysical model permits the retrieval of microphysical parameters corresponding to some average cloud microphysical characteristics that will lead to realistic optical behavior of the cloud. Therefore the retrieved optical parameters must be compared to measurements or to more realistic modeling.

[45] For liquid-water clouds (Table 2), the mean value of the asymmetry parameter $g = 0.848$ at $\lambda = 0.8$ μm is typical of water droplet clouds [*Raga and Jonas*, 1993] and in good agreement with the value of 0.844 or 0.835 derived from the observational studies at $\lambda = 0.635$ μm made by *Gerber et al.* [2000] using the Cloud-Integrating Nephelometer (CIN) in stratocumulus clouds. This difference in wavelength is not significant to affect the value of the asymmetry parameter. *Gayet et al.* [2002a] displayed a vertical profile of the extinction coefficient for typical liquid stratocumulus clouds using FSSP measurements and the Polar Nephelometer data at $\lambda = 0.8$ μm. They have obtained mean values of the water-droplet-effective radii of around 6 or 7 μm. The corresponding single-scattering albedo and asymmetry parameter can be determined using Mie theory and assuming a lognormal water droplet spectra with an effective radius of 6.5 μm. We have found, $\omega_{sca} = 1.000$, 0.995, and 0.930, and $g = 0.849$, 0.815, and 0.754 for $\lambda = 0.8$, 1.6, and 3.7 μm, respectively. Measurements of the extinction coefficient at $\lambda = 0.8$ μm between the altitudes of 1000 and 1500 m correspond to values ranging from 20 to 60 km^{-1}. All these single-scattering parameters are comparable to the coefficients presented in Table 2.

Table 3. Same as Table 2 but for Mixed-Phase Cloud

Mixed-Phase Clouds	Mean Value	Lowest Value	Highest Value
	$\lambda = 0.8$ μm		
Extinction: σ_{ext}, km^{-1}	8.974	4.245	18.970
Albedo: ω_{sca}	1.000	1.000	1.000
Asymmetry: g	0.8012	0.7070	0.8040
	$\lambda = 1.6$ μm		
Extinction: σ_{ext}, km^{-1}	10.377	4.795	22.462
Albedo: ω_{sca}	0.9937	0.9925	0.9947
Asymmetry: g	0.8006	0.7972	0.8044
	$\lambda = 3.7$ μm		
Extinction: σ_{ext}, km^{-1}	10.354	4.559	23.511
Albedo: ω_{sca}	0.9512	0.9447	0.9579
Asymmetry: g	0.7927	0.7855	0.8001

[46] Even though mixed-phase clouds represent an important group of atmospheric clouds, references on the scattering behavior of these clouds are hard to find. The main problem is how to distinguish a mixed-phase cloud from a mostly liquid-water cloud or a solid-ice cloud. We have chosen to define mixed-phase clouds as clouds whose scattering behaviors are intermediate between liquid-water clouds and solid-ice clouds. This is possible by using the method developed by *Jourdan et al.* [2003]. The identification of mixed-phase clouds on the base of their side scattering differences with water or ice clouds was also proposed by *Sassen and Liou* [1979]. In the work of *Garret et al.* [2001], measurements of asymmetry parameter and extinction coefficient as a function of ice particle number concentration in stratocumulus clouds have been performed. The authors showed that the values of the asymmetry parameter vary linearly from 0.87 for clouds containing no ice to 0.73 for completely glaciated clouds at a wavelength of 0.635 μm. For intermediate values of the ice particle fraction (i.e., number of ice particles/(number of ice particles + number of water drops)), corresponding to mixed-phase clouds, the asymmetry parameter and the extinction coefficient are approximately equal to 0.80 ± 0.02 and (15 ± 10) km^{-1}. These estimations, especially for the g value, are in agreement with the results presented in Table 3 for a wavelength of 0.8 μm. These comparisons can only be done qualitatively since the ice particle fractions calculated using the microphysical parameters of Table 1 and the ones presented by Garret et al. are not directly comparable. Furthermore, the mean value of the extinction coefficient measured in typical mixed-phase stratocumulus, at a wavelength of 0.8 μm, by *Gayet et al.* [2002a] is (10 ± 4) km^{-1}, and the distribution of the asymmetry parameter exhibits two modes centered around 0.835 and 0.79. The mode with a g value of 0.835 corresponds to a small number of water

droplets dominating the optical properties. The other mode includes higher concentration of ice crystals such as pristine-dentric-shaped and some aggregates characterized by a g value of 0.79, which is close to the mean asymmetry parameter presented in Table 3 for mixed-phase clouds.

[47] Appropriate assessment of ice cloud optical properties is currently an open question. Specifically, the asymmetry parameter and phase function were theoretically calculated for different single ice crystal shapes and predicted g values between 0.74 (even as small as 0.69 for ice crystals with multiple internal inclusions of air bubbles [*Macke*, 2000]) and 0.95 at nonabsorbing wavelength [*Iaquinta et al.*, 1995; *Macke et al.*, 1996; *Yang and Liou*, 1998; *Francis et al.*, 1999]. Moreover, optical parameters of ice clouds can also be derived from measurements of radiance fields in cirrus clouds or calculated from measured cloud structure (particle size distribution, ice crystal shape). The value of the asymmetry parameter inferred from observational studies lies between 0.70 [*Stephens et al.*, 1990] and 0.85 [*Francis et al.*, 1999] (*Macke et al.* [1998] even found g values of 0.91 for midlatitude cirrus constituted of hexagonal plates). In cirrus clouds, values of the extinction coefficient inferred by 2D-C particle size distribution measurements were evaluated between 0.2 and 2.0 km^{-1} for nonabsorbing wavelength [*Kinne et al.*, 1997; *Macke et al.*, 1998; *Yang and Liou*, 1998]. Finally, the asymmetry parameter and extinction coefficient can be estimated. From laboratory measurements, *Volkovitsky et al.* [1979] and *Sassen and Liou* [1979] found g values near 0.83 ± 0.02. Nevertheless, the measurements concerned only a scattering phase function from 10° to 175°, leading to possible erroneous calculation of the corresponding asymmetry parameter. In situ measurements performed by a cloud-integrating nephelometer [*Gerber et al.*, 2000; *Garret et al.*, 2001] in Arctic clouds and the Polar Nephelometer [*Auriol et al.*, 2001] in cirrus clouds gave g values ranging from 0.73 to 0.79 and σ_{ext} ranging from 1.5 to 14.5 km^{-1}. Furthermore, *Korolev et al.* [2001] measured extinction coefficient for glaciated clouds around 2 km^{-1}, and even though *Gerber et al.* [2000] suggested that a typical asymmetry value for ice clouds could be 0.73, their average value over all glaciated clouds came out to be 0.82.

[48] As noted above, the ice clouds that are described in this paper consist of different types of ice clouds (cirrus, cirro-stratus, glaciated strato-cumulus, alto-cumulus), whereas most of the cloud optical properties available in the literature correspond to cirrus clouds specifically. Therefore a cirrus cloud class has been extracted from the glaciated class on the basis of temperature regimes. Glaciated clouds are considered to be cirrus clouds when their temperature is lower than −40°C.

[49] The retrieved particle size distributions are displayed in Figure 1d, and the angular scattering coefficients at the three wavelengths are presented in Figures 2d, 2h, and 2l. For cirrus clouds, the water-droplet contribution is less important than for glaciated clouds, and even though the 22° and 46° halos are sharper, the angular scattering coefficient still exhibits rather smooth behavior which is consistent with the observations in cirrus clouds for nonabsorbing wavelength [*Auriol et al.*, 2001].

[50] The typical average angular scattering coefficient shown in Figure 6 (at 0.8 μm) is in agreement with

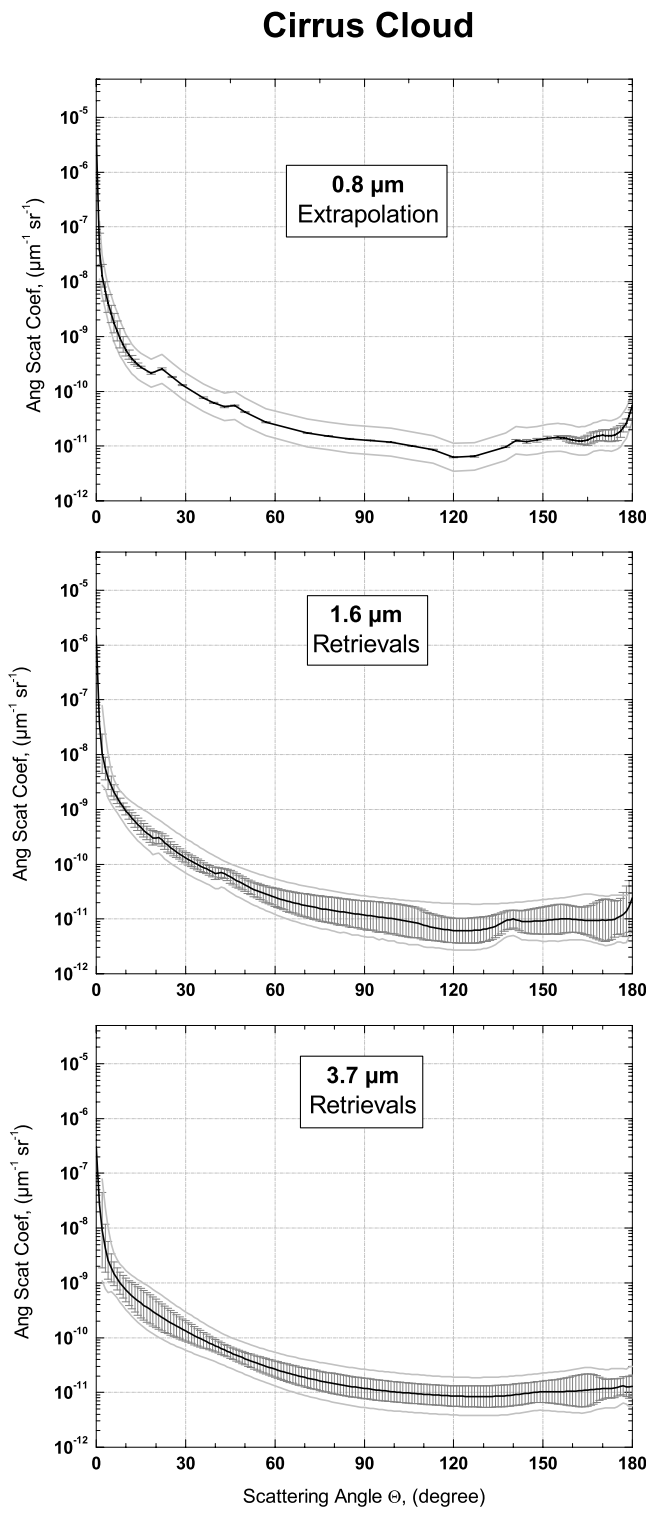

Figure 6. Same as in Figure 3 but for cirrus cloud.

definition of *Baran et al.* [2001]. Indeed, they argued that an appropriate phase function for cirrus clouds should be one which is generally smooth, featureless, and represents angular scattering from a collection of various shape of particles. Moreover, the inferred microphysical parameters displayed in Table 1 for the cirrus case compare well with the measurements performed by *Korolev et al.* [2001], who assessed values for concentration and total water content of

Table 4. Same as Table 2 but for Ice Crystal Cloud (Glaciated Cloud)

Solid-Ice Clouds	Mean Value	Lowest Value	Highest Value
	$\lambda = 0.8$ μm		
Extinction: σ_{ext}, km^{-1}	1.921	0.730	5.052
Albedo: ω_{sca}	0.9999	0.9998	0.9999
Asymmetry: g	0.8142	0.8131	0.8153
	$\lambda = 1.6$ μm		
Extinction: σ_{ext}, km^{-1}	1.752	0.666	4.607
Albedo: ω_{sca}	0.9451	0.9206	0.9705
Asymmetry: g	0.8216	0.8018	0.8418
	$\lambda = 3.7$ μm		
Extinction: σ_{ext}, km^{-1}	1.603	0.555	4.631
Albedo: ω_{sca}	0.7866	0.7370	0.8393
Asymmetry: g	0.8018	0.7746	0.8299

5 cm^{-3} and 0.01 g m^{-3}, respectively. Observations during the Interhemispheric differences in Cirrus properties from Anthropogenic emissions (INCA) campaign led to values of effective radius close to 25 or 30 μm, an extinction coefficient of 0.5 km^{-1}, and an asymmetry parameter ranging from 0.77 to 0.79 at visible wavelengths [*Gonzalez et al.*, 2002]. These measurements are completely in accordance with those we have retrieved for cirrus clouds (Table 5).

[51] As a whole, the values of the asymmetry parameter and the extinction coefficient presented in Table 4 (glaciated clouds) and specially in Table 5 (cirrus clouds) at nonabsorbing wavelengths are consistent with the values established by previous studies. As one can see, the asymmetry parameter and the extinction coefficient have lower values for cirrus clouds than for glaciated clouds. It is rather difficult, however, to extract representative values of optical parameters, in particular for the value of g, which best represents glaciated clouds.

[52] Information at absorbing wavelengths (1.6 and 3.7 μm) is useful to conclude on the reliability of our results. The wavelength of 0.8 μm gives information on the optical thickness (extinction coefficient), while wavelengths of 1.6 and 3.7 μm are sensitive to the ice crystal dimension. Therefore the single-scattering albedo and asymmetry parameter at different wavelengths are particularly sensitive to the size and shape of ice crystals [*Hess and Wiegner*, 1994].

[53] We have calculated the single-scattering albedo and asymmetry parameter for various ice crystal habits at the three wavelengths using the database described by *Yang et al.* [2000] and *Key et al.* [2002]. For four-branch bullet rosettes, the same kind of scattering behavior is observed, as shown in Table 4. Indeed, at $\lambda = 0.8$ μm and for an effective radius around 25 μm, computations give $g = 0.808$ and $\omega_{sca} = 1.000$; at $\lambda = 1.6$ μm, $g = 0.815$ and $\omega_{sca} = 0.961$; at $\lambda = 3.7$ μm, $g = 0.800$ and $\omega_{sca} = 0.780$. Calculations were also performed for rough aggregates, with an effective radius of 35 μm, and compared to the optical parameters retrieved for the cirrus cloud case. The following parameters were obtained: $g = 0.770$ and $\omega_{sca} = 1.000$; at $\lambda = 1.6$ μm, $g = 0.794$ and $\omega_{sca} = 0.954$; at $\lambda = 3.7$ μm, $g = 0.860$ and $\omega_{sca} = 0.700$. These simulations fit with our retrievals except for strongly absorbing wavelengths (3.7μm), where most of the errors are made in our inversion scheme.

[54] *Baran et al.* [2001] proposed a parameterization of the Henyey-Greenstein scattering phase function, for application to satellite remote sensing and aircraft observations of cirrus, based on a nonabsorbing-laboratory-measured phase function between the scattering angles of 30° and 180°. This analytical phase function reproduced well both aircraft and satellite measurements in cirrus clouds. The corresponding best fit of scattering properties for an effective radius of 25 μm was $g(0.87\ \mu m) = 0.80$, $\omega_{sca}(0.87\ \mu m) = 1.000$; $g(1.6\ \mu m) = 0.81$, $\omega_{sca}(1.6\ \mu m) = 0.921$; $g(3.7\ \mu m) = 0.84$, $\omega_{sca}(3.7\mu m) = 0.742$. These values are in agreement with those we found, at least at 0.8 and 1.6 μm, for cirrus clouds. The observed discrepancies, especially at 3.7μm, could come from the errors caused by the inverse model and they could also be attributed to the fact that the transmittance measurements by *Baran et al.* [2001] were not available under 10°.

[55] A final point to be emphasized is that the uncertainties in both extrapolated angular scattering coefficient and reproduction of all single light-scattering characteristics in the infrared region increase as the fraction of ice increases. The tendency could be explained by the fact that the size of ice crystals considerably exceeds the size of water droplets as a whole. Thus the sensitivity of light-scattering properties becomes higher for both the forward scattering directions and infrared region, which are not available from the initial Polar Nephelometer measurements used in this study. Accordingly, the Polar Nephelometer probe should be improved in order to bring more information, especially in the forward scattering direction where the size effect is gathered. This would allow for a more accurate retrieval of particle size distributions and thus scattering phase functions at different wavelengths with less uncertainties.

5. Conclusions and Outlook

[56] In this paper, a measured set of approximately 60,000 airborne angular scattering coefficients were involved to reproduce a complete representative set of both microphysical parameters and single light-scattering characteristics at wavelengths 0.8, 1.6, and 3.7 μm. On the basis of the statistical classification approach and inversion method, for each cloud's phase, the information contained in the average angular scattering coefficients measured at the wavelength 0.8 μm and scattering angles 15°–155° was extrapolated to the forward and backward scattering directions. Therefore this enabled us to establish complete scatter-

Table 5. Same as Table 2 but for Cirrus Cloud

Cirrus Clouds	Mean Value	Lowest Value	Highest Value
	$\lambda = 0.8$ μm		
Extinction: σ_{ext}, km^{-1}	0.855	0.476	1.536
Albedo: ω_{sca}	0.9999	1.0000	0.9993
Asymmetry: g	0.7888	0.7870	0.7909
	$\lambda = 1.6$ μm		
Extinction: σ_{ext}, km^{-1}	0.905	0.503	1.629
Albedo: ω_{sca}	0.9542	0.9457	0.9632
Asymmetry: g	0.8059	0.7986	0.8128
	$\lambda = 3.7$ μm		
Extinction: σ_{ext}, km^{-1}	0.887	0.475	1.656
Albedo: ω_{sca}	0.8245	0.8016	0.8478
Asymmetry: g	0.7570	0.7457	0.7684

ing phase functions for wavelengths 0.8, 1.6, and 3.7 μm. For each type of cloud, the inferred scattering phase function is presented in terms of total angular scattering coefficient as well as a combination of a water droplet component and hexagonal ice crystal component. Additionally, the average microphysical and integral optical parameters were calculated for each cloud category.

[57] Possible variations in the retrieved parameters are presented separately due to both random instrumental errors of optical measurements and possible changes in the microphysical parameters within a separated specific cloud category. The microphysical parameter retrievals are validated by comparison with collocated direct particle size distribution measurements. Additionally, the estimated single light-scattering characteristics agree well enough with those available from the literature.

[58] The retrieved microphysical and optical parameters could be of great interest for further cloud characterization in radiative direct and inverse modeling (they are available at the following Internet address: www.obs.univ-bpclermont.fr/atmos/nephelo/ or by email upon request). The next step of the study should include the parameters in the appropriate radiative transfer models by setting up the corresponding representative lookup table needed for both climate modeling and remote sensing. Finally, we plan to incorporate additional parameters into the inverse model, which are capable of retrieving ice crystal inhomogeneity or surface roughness. However, large sets of numerical simulations must be performed in order to check if the requirements imposed by the light-scattering measurements are consistent with the additional degrees of freedom in the inverse model produced by a more sophisticated microphysical model.

Appendix A: Estimation of the Impact of Instrumental Errors and Variation of Microphysical Parameters on the Retrievals

[59] The covariance matrix of the retrieved particle size distributions satisfies the following equation [*Tarantola*, 1994]:

$$\mathbf{C}_{\varphi} = \left(\mathbf{K}^{\mathrm{T}}\mathbf{C}_{\sigma}^{-1}\mathbf{K} + \mathbf{\Omega}\right)^{-1}, \tag{A1}$$

where $\mathbf{C}_{\sigma}$ is the covariance matrix of the measured data, T denotes matrix transposition, and $\mathbf{\Omega}$ is the smoothness matrix. For a two-desired phase case, $\mathbf{\Omega}$ consists of two diagonal blocks

$$\mathbf{\Omega} = \begin{bmatrix} \Omega_1 & 0 \\ 0 & \Omega_2 \end{bmatrix},$$

each corresponding to the smoothness matrices of water droplet and ice crystal components, respectively (the smoothness parameters are included into the matrices). The covariance matrix $\mathbf{C}_{\gamma}$ of a set of L estimated characteristics γ_l (l = 1,2,. . .,L) from the retrieved particle size distribution $\hat{\varphi}$, with $\hat{\gamma} = \mathbf{G}\hat{\varphi}$ can be computed when $\mathbf{C}_{\varphi}$ is known [*Rao*, 1973]:

$$\mathbf{C}_{\gamma} = \mathbf{G}\mathbf{C}_{\varphi}\mathbf{G}^{\mathrm{T}} = \mathbf{G}\left(\mathbf{K}^{\mathrm{T}}\mathbf{C}_{\sigma}^{-1}\mathbf{K} + \mathbf{\Omega}\right)^{-1}\mathbf{G}^{\mathrm{T}}. \tag{A2}$$

Equations (10) and (A2) can be used directly to obtain both average angular scattering coefficients (within the scattering angles 0°–180°) and their possible variations at the three desired wavelengths.

[60] In processing of statistical data, the covariance matrix $\mathbf{C}_{\sigma}$ could consist of at least two kinds of variations. The first is caused by random instrumental error of optical measurements. The second variation could have physical nature associated with changing of microphysical parameters within a certain separated specific cloud category (i.e., liquid, mixed, or ice phase). We have studied both effects on the retrievals.

[61] The quality of the computed optical properties is evidently determined by the quality in retrieving the size composition. This problem, however, has particular features of its own. To gain a better understanding of the distinctive features of this task, let us present the diagonal elements of matrix $\mathbf{C}_{\gamma}$ in the context of sensitivity effects of both measured and retrieved optical properties to primarily parameters as well as through correlations of these sensitivities. Assuming for simplicity sake that $\mathbf{\Omega} = 0$ and that the covariance matrix of initial measurements has diagonal structure with the same values of diagonal elements C_{σ}, one can write

$$\left\{C_{\gamma}\right\}_{ll} = C_{\sigma} \times \sum_{j} \frac{\left(\mathbf{G}_l\mathbf{G}_l^{\mathrm{T}}\right)}{\left(\mathbf{K}_j\mathbf{K}_j^{\mathrm{T}}\right)} \times \frac{1 - \rho^2_{\gamma_l,\sigma_1\ldots\sigma_{j-1}\sigma_{j+1}\ldots\sigma_J}}{1 - \rho^2_{\sigma_j,\sigma_1\ldots\sigma_{j-1}\sigma_{j+1}\ldots\sigma_J}}. \tag{A3}$$

[62] In equation (A3), $\mathbf{K}_j$ and $\mathbf{G}_l$ are vector rows of matrices $\mathbf{K}$ and $\mathbf{G}$ with indexes j and l, respectively, the norms $\mathbf{K}_j\mathbf{K}_j^{\mathrm{T}}$ and $\mathbf{G}_l\mathbf{G}_l^{\mathrm{T}}$ characterize the total sensitivity of characteristics σ_j and γ_l to all primary parameters φ_i. The value of $\rho_{\sigma_j,\sigma_1\ldots\sigma_{j-1}\sigma_{j+1}\ldots\sigma_J}$ is the multiple correlation coefficient between the vector-row $\mathbf{K}_j$ and all other rows of matrix $\mathbf{K}$ which is responsible for the conditioning of this matrix $\mathbf{K}\mathbf{K}^{\mathrm{T}}$ in the inverse problem. The value of $\rho_{\beta_l,\sigma_1\ldots\sigma_{j-1}\sigma_{j+1}\ldots\sigma_J}$ is the multiple correlation coefficient between the vector-row $\mathbf{G}_l$ and the rows of matrix $\mathbf{K}$ with the vector-row $\mathbf{K}_j$ removed. In geometrical interpretation, $\rho_{\sigma_j,\sigma_1\ldots\sigma_{j-1}\sigma_{j+1}\ldots\sigma_J}$ or $\rho_{\gamma_l,\sigma_1\ldots\sigma_{j-1}\sigma_{j+1}\ldots\sigma_J}$ constitute the cosines of the angles between $\mathbf{K}_j$ or $\mathbf{G}_l$, respectively, and the hyperplane generated by all other vector-rows $\mathbf{K}_1$, $\mathbf{K}_2$,. . ., $\mathbf{K}_{j-1}$, $\mathbf{K}_{j+1}$,. . ., $\mathbf{K}_J$. It is quite natural from equation (A3) that the error variance in estimating γ_l characteristics falls off with increasing the sensitivity of initial measurements to φ_i and with decreasing the sensitivity of γ_l to these parameters. At the same time, the error variance could be also significantly decreasing under high correlation between rows σ_j and γ_l ($\rho^2_{\gamma_l,\sigma_1\ldots\sigma_{j-1}\sigma_{j+1}\ldots\sigma_J} \rightarrow 1$). This is the main distinctive feature in retrieving the desired characteristics γ_l.

[63] **Acknowledgments.** We are very grateful to J. F. Fournol, C. Duroure, F. Auriol, O. Crépel and L. Cortès for their helpful collaboration in the field experiments. The ARAT'97 experiment was funded under grants from DRET contract 9634104 and from the PATOM Committee (CNRS/INSU). The CIRRUS'98 experiment was supported by the French DSP/STTC (Direction des systèmes de forces et de la Prospective/Service Technique des Technologies Communes) within the ONERA contract 23.140/DA.B1/BC. The JACCS program is supported by the Science and Technology Agency of Japanese Government. The authors thank Douglas Orsini and the two anonymous reviewers for their help in improving the manuscript.

References

Asano, S., A. Uchiyama, A. Yamazaki, J. F. Gayet, and M. Tanizono, Two case studies of winter continental-type water and mixed-phased stratocumuli over the sea: 2. Absorption of solar radiation, *J. Geophys. Res.*, *107*(D21), 4570, doi:10.1029/2001JD001108, 2002.

Auriol, F., J. F. Gayet, G. Febvre, O. Jourdan, L. Labonnote, and G. Brogniez, In situ observations of cirrus cloud scattering phase function with 22° and 46° halos: Cloud field study on 19 February 1998, *J. Atmos. Sci.*, *58*, 3376–3390, 2001.

Baran, A. J., P. N. Francis, L. C. Labonnote, and M. Doutriaux-Boucher, A scattering phase function for ice cloud: Tests of applicability using aircraft and satellite multi-angle multi wavelength radiance measurements of cirrus, *Q. J. R. Meteorol. Soc.*, *127*, 2395–2416, 2001.

Crépel, O., J. F. Gayet, J. F. Fournol, and S. Oshchepkov, A new airborne Polar Nephelometer for the measurements of optical and microphysical cloud properties, *Ann. Geophys.*, *15*, 451–459, 1997.

Durand, G., J. F. Gayet, L. Kaës, and P. Matharan, Airborne infrared and microphysical measurements on cirrus clouds, *SPIE Int. Soc. Opt. Eng.*, *3495*, 72–81, 1998.

Duroure, C., F. Auriol, O. Crepel, and J.-F. Gayet, Microscale inhomogeneities study using high resolution Polar Nephelometer measurements, paper presented at XXIII General Assembly, European Geophysical Society, Nice, France, April 20–24 , 1998.

Francis, P. N., J. S. Foot, and A. J. Baran, Aircraft measurements of the solar and infrared radiative properties of cirrus and their dependence on ice crystal shape, *J. Geophys. Res.*, *104*, 31,685–31,695, 1999.

Garret, T. J., P. V. Hobbs, and H. Gerber, Shortwave, single-scattering properties of Arctic ice clouds, *J. Geophys. Res.*, *106*, 15,155–15,172, 2001.

Gayet, J. F., G. Febvre, G. Brogniez, H. Chepfer, W. Renger, and P. Wendling, Microphysical and optical properties of cirrus and contrails: Cloud field study on 13 October 1989, *J. Atmos. Sci.*, *53*, 126–138, 1996.

Gayet, J. F., F. Auriol, S. L. Oshchepkov, F. Schröder, C. Duroure, G. Febvre, J. F. Fournol, O. Crépel, P. Personne, and D. Daugeron, In situ optical and microphysical measurements with a new airborne ''Polar Nephelometer'', *Geophys. Res. Lett.*, *25*, 971–974, 1997.

Gayet, J. F., S. Asano, A. Yamazaki, A. Uchiyama, A. Sinyuk, O. Jourdan, and F. Auriol, Two case studies of continental-type water and maritime mixed-phased stratocumuli over the sea: 1. Microphysical and optical properties, *J. Geophys. Res.*, *107*(D21), 4569, doi:10.1029/2001JD001106, 2002a.

Gayet, J. F., F. Auriol, A. Minikin, J. Ström, M. Seifert, R. Krejci, A. Petzol, G. Febvre, and U. Schumann, Quantitative measurement of microphysical and optical properties of cirrus clouds with four different in situ probes: Evidence of small ice crystals, *Geophys. Res. Lett.*, *29*(24), 2230, doi:10.1029/2001GL014342, 2002b.

Gerber, H., Y. Takano, T. J. Garrett, and P. V. Hobbs, Nephelometer measurements of the asymmetry parameter, volume extinction coefficient and backscatter ratio in Arctic clouds, *J. Atmos. Sci.*, *57*, 3021–3034, 2000.

Gonzales, A., P. Wendling, B. Mayer, J. F. Gayet, and T. Rother, Remote sensing of cirrus cloud properties in presence of lower clouds: An ATSR-2 case study during INCA, *J. Geophys. Res.*, *107*(D23), 4693, doi:10.1029/2002JD002535, 2002.

Hess, M., and M. Wiegner, COP: A data library of optical properties of hexagonal ice crystals, *Appl. Opt.*, *33*, 7740–7746, 1994.

Hess, M., R. B. A. Koelemeijer, and P. Stammes, Scattering matrices of imperfect hexagonal ice crystals, *J. Quant. Spectrosc. Radiat. Transfer*, *60*, 301–308, 1998.

Iaquinta, J., H. Isaka, and P. Personne, Scattering phase function of bullet rosette ice crystals, *J. Atmos. Sci.*, *52*, 1401–1413, 1995.

Jourdan, O., S. L. Oshchepkov, J. F. Gayet, V. N. Shcherbakov, and H. Isaka, Statistical analysis of cloud light scattering and microphysical properties obtained from airborne measurements, *J. Geophys. Res.*, *108*(D5), 4155, doi:10.1029/2002JD002723, 2003.

Key, J., P. Yang, B. Baum, and S. Nasiri, Parameterization of shortwave ice cloud optical properties for various particle habits, *J. Geophys. Res.*, *107*(D13), 4181, doi:10.1029/2001JD000742, 2002.

Kinne, S., T. P. Ackerman, A. J. Heymsfield, F. P. J. Valero, K. Sassen, and J. D. Spinhirne, Cirrus microphysics and radiative transfer: Cloud field study on 28 October 1986, *Mon. Weather Rev.*, *20*, 661–684, 1992.

Kinne, S., T. P. Ackerman, M. Shiobara, A. Uchiyama, A. J. Heymsfield, L. Miloshevich, J. Wendell, E. W. Eloranta, C. Purgold, and R. W. Bergstrom, Cirrus cloud radiative and microphysical properties from ground observations and in situ measurements during FIRE 1991 and their application to exhibit problems in cirrus solar radiative modeling, *J. Atmos. Sci.*, *54*, 2320–2344, 1997.

Knollenberg, R. G., Techniques for probing cloud microstructure, in *Clouds, Their Formation, Optical Properties and Effects*, edited by P. V. Hobs and A. Deepak, pp.15–92, Academic, San Diego, Calif., 1981.

Korolev, A. V., G. A. Isaac, I. P. Mazin, and H. W. Barker, Microphysical properties of continental stratiform clouds, *Q. J. R. Meteorol. Soc.*, *121*, 2117–2151, 2001.

Labonnote, L. C., G. Brogniez, M. Doutriaux-Boucher, J. C. Buriez, J. F. Gayet, and H. Chepfer, Modeling of light scattering in cirrus clouds with inhomogeneous hexagonal monocrystals: Comparison with in-situ and ADEOS-POLDER measurements, *Geophys. Res. Lett.*, *27*, 113–116, 2000.

Lacis, A. A., and M. I. Mishchenko, Climate forcing, climate sensitivity, and climate response: A radiative modeling perspective on atmospheric aerosols, in *Aerosol Forcing of Climate: Report of the Dahlem Workshop on Aerosol Forcing of Climate*, edited by R. J. Charlson and J. Heintzenberg, John Wiley, Hoboken, N. J., 1995.

Liou, K. N., and Y. Takano, Light scattering by nonspherical particles: Remote sensing and climatic implications, *Atmos. Res.*, *31*, 271–298, 1994.

Liou, K. N., Y. Takano, and P. Yang, Light scattering and radiative transfer in ice crystal clouds: Applications to climate research, in *Light Scattering by Nonspherical Particles: Theory, Measurements and Geophysical Applications*, edited by M. I. Mishchenko, J. W. Hovenier, and L. D. Travis, chap. 15, 418–449, Academic, San Diego, Calif., 2000.

Macke, A., Monte Carlo calculations of light scattering by large particles with multiple internal inclusions, in *Light Scattering by Nonspherical Particles: Theory, Measurements and Geophysical Applications*, edited by M. I. Mishchenko, J. W. Hovenier, and L. D. Travis, chap. 10, 309–322, Academic, San Diego, Calif., 2000.

Macke, A., J. Mueller, and E. Raschke, Single-scattering properties of atmospheric ice crystals, *J. Atmos. Sci.*, *53*, 2813–2825, 1996.

Macke, A., P. N. Francis, G. M. McFarquhar, and S. Kinne, The role of ice particle shapes and size distributions in the single-scattering properties of cirrus clouds, *J. Atmos. Sci.*, *55*, 2874–2883, 1998.

Mishchenko, M. I., and L. D. Travis, Electromagnetic scattering by nonspherical particles, in *Exploring the Atmosphere by Remote Sensing Techniques*, pp. 77–127, Springer-Verlag, New York, 2003.

Mishchenko, M. I., W. J. Wiscombe, J. W. Hovenier, and L. D. Travis, Overview of scattering by nonspherical particles, in *Light Scattering by Nonspherical Particles: Theory, Measurements and Geophysical Applications*, edited by M. I. Mishchenko, J. W. Hovenier, and L. D. Travis, chap. 2, pp. 29–60, Academic, San Diego, Calif., 2000.

Oshchepkov, S. L., and H. Isaka, Inverse scattering problem for mixed-phase and ice clouds, part 1, Numerical simulation of particle sizing from phase function measurements, *Appl. Opt.*, *36*, 8765–8774, 1997.

Oshchepkov, S. L., H. Isaka, J. F. Gayet, A. Sinyuk, F. Auriol, and S. Havemann, Microphysical properties of mixed-phase & ice clouds retrieved from in situ airborne ''Polar Nephelometer'' measurements, *Geophys. Res. Lett.*, *27*, 209–213, 2000.

Raga, G. B., and P. R. Jonas, Microphysical and radiative properties of small cumulus clouds over the sea, *Q. J. R. Meteorol. Soc.*, *119*, 1399–1417, 1993.

Ramanathan, V., R. D. Cess, E. F. Harrison, P. Minnis, B. R. Backstrom, E. Ahmad, and D. Hartmann, Cloud-radiative forcing of climate: Results from the Earth radiation budget experiment, *Science*, *243*, 57–63, 1989.

Rao, C. R., *Linear Statistical Inference and Its Applications*, 2nd ed., 656 pp., John Wiley, Hoboken, N. J., 1973.

Rossow, W. B., and R. A. Schiffer, ISCCP cloud data products, *Bull. Am. Meteorol. Soc.*, *72*, 2–20, 1991.

Rossow, W. B., and R. A. Schiffer, Advances in understanding clouds from ISCCP, *Bull. Am. Meteorol. Soc.*, *80*, 2261–2288, 1999.

Sassen, K., and K. N. Liou, Scattering and polarized laser light by water droplets, mixed-phase and ice crystal clouds, part I, Angular scattering patterns, *J. Atmos. Sci.*, *36*, 838–851, 1979.

Stephens, G. L., S. C. Tsay, P. W. Stackhouse, and P. J. Flatau, The relevance of microphysical and radiative properties of cirrus clouds to climate and climate feedback, *J. Atmos. Sci.*, *47*, 1742–1753, 1990.

Takano, Y., and K. N. Liou, Solar radiative transfer in cirrus clouds, part I, Single-scattering and optical properties of hexagonal ice crystals, *J. Atmos. Sci.*, *46*, 3–18, 1989.

Tarantola, A., *Inverse Problem Theory: Model for Data Fitting and Model Parameter Estimation*, 1st ed., 601 pp., Elsevier Sci., New York, 1994.

Twomey, S., *Introduction to the Mathematics of Inversion in Remote Sensing and Indirect Measurements*, 243 pp., Elsevier Sci., New York, 1977.

Volkovitsky, O. A., L. N. Pavlova, and A. G. Petrushin, Scattering of light by ice crystals, *Atmos. Ocean Phys.*, *16*, 90–102, 1979.

Yang, P., and K. N. Liou, Geometric-optics-integral-equation method for light scattering by nonspherical ice crystals, *Appl. Opt.*, *35*, 6568–6584, 1996.

Yang, P., and K. N. Liou, Single-scattering properties of complex ice crystals in terrestrial atmosphere, *Contrib. Atmos. Phys.*, *71*, 223–248, 1998.

Yang, P., K. N. Liou, K. Wyser, and D. Mitchell, Parameterization of scattering and absorption properties of individual ice crystals, *J. Geophys. Res.*, *105*, 4699–4718, 2000.

J.-F. Gayet, H. Isaka, O. Jourdan, S. Oshchepkov, and V. Shcherbakov, Laboratoire de Météorologie Physique (LaMP), Université Blaise Pascal, UMR/CNRS 6016, 24, avenue des Landais, 63177 Aubiere Cedex, Clermont-Ferrand, France. (o.jourdan@opgc.univ-bpclermont.fr)